Journal of Applied Fluid Mechanics, Vol. 18, No. 9, pp. 2421-2433, 2025.
Available online at www.jafmonline.net, ISSN 1735-3572, EISSN 1735-3645.
https://doi.org/10.47176/jafm.18.9.3233

Study on the Effect of Floating Impeller Axial Displacement on the Performance and Axial Force of Vortex Pumps

W. F. Yang[1], R. H. Zhang[1,2,3†], X. Y. Wang[1] and G. Q. Guo[1,2,3]

[1] *School of Energy and Power Engineering, Lanzhou University of Technology, Lanzhou, Gansu Province, 730050, China*
[2] *Key Laboratory of Advanced Pumps, Valves and Fluid Control System of the Ministry of Education, Lanzhou University of Technology, Lanzhou, Gansu Province, 730050, China*
[3] *Key Laboratory of Fluid Machinery and Systems, Lanzhou, Gansu Province, 730050, China*

†*Corresponding Author Email: zhangrh@lut.edu.cn*

ABSTRACT

The impact of the axial displacement of a floating impeller in a vortex pump on performance and axial force was investigated through numerical simulations, validated by experimental tests. Simulations were conducted to calculate axial forces at various impeller positions under different operating conditions. The results indicate that increasing the axial displacement of the impeller reduces both the pump head and efficiency. Compared with inlet axial clearance, reducing the outlet axial clearance improves energy conversion while having a smaller effect on head performance. At lower flow rates, the pressure difference between the balance cavities on both sides of the floating impeller increases, leading to a higher axial force. Adjusting the axial position of the impeller can effectively reduce axial force, optimising both its magnitude and direction to help restore the impeller to a central position. The balance cavity modifies the static pressure distribution in the high-pressure region of the impeller, further minimising extreme axial force values in this region. However, as flow rate increases, the influence of the balance cavity diminishes.

Article History

Received November 1, 2024
Revised April 2, 2025
Accepted April 15, 2025
Available online July 5, 2025

Keywords:

Vortex pump
Floating impeller
Axial displacement
Performance
Axial force

1. INTRODUCTION

As a low-specific-speed vane pump, the vortex pump offers advantages such as a low flow rate, high head, strong self-priming capability, and the ability to transport gas-liquid mixtures. It is widely used in critical industries, including petrochemical, aerospace, shipping, and automotive sectors (Raheel & Engeda, 2005; Guan, 2011).

The clearance between the impeller and casing plays a crucial role in vortex pump performance. To minimise liquid leakage from high- to low-pressure regions, the axial clearance in vortex pumps is typically kept between 0.1 and 0.25 mm. In vortex pumps with single-sided flow channels, the differing static pressures on the impeller end faces generate an axial force directed toward the flow channel (Jia, 1993). In pumps equipped with hydraulic balance devices, variable working conditions can lead to impeller end-face wear and even impeller jamming due to unbalanced axial forces, potentially resulting in motor overload and operational failure.

Research on the axial force of floating impellers has predominantly focused on centrifugal pumps (Gantar et al., 2002; Liu et al., 2013, 2014, 2015; Wang et al., 2024), while studies on axial forces in single-sided flow-channel vortex pumps remain limited. Zhao et al. (2013) examined the effect of wear ring clearance variations on axial force in centrifugal pumps and found that front wear ring clearance exhibited the most significant impact. Pehlivan and Parlak (2019) conducted a CFD analysis of axial load parameters in a single-suction closed-impeller centrifugal pump, concluding that the wear-resistant ring and balance hole significantly influenced axial load, whereas the back clearance of the impeller had minimal effect. Adu-Poku et al. (2022) employed numerical methods to examine pressure fluctuation intensity in the clearance of vortex pumps, characterizing axial and radial force distributions around the impeller under different blade suction angles. Chen et al. (2022a) explored how flow in the front and rear cavities of a multistage centrifugal pump affects axial force, identifying the leakage direction in the pump chamber and rotation effects in the core area as key factors.

Zeng et al. (2022) developed a mathematical model for pressure distribution in the impeller cover's side cavity, incorporating various radial clearances of the

NOMENCLATURE

b	blade width	H	pump head
b_1	designed inlet axial clearance	n_0	rotational speed
b_2	designed outlet axial clearance	p	static pressure
d_1	inlet axial clearance	Q_0	nominal flow rate of pump
d_2	outlet axial clearance	Q	flow rate
D_1	impeller inner diameter	u_2	circumferential velocity at the impeller outlet
D_2	impeller outer diameter	Z	blade number
D_3	side channel inner diameter	ζ_D	loss coefficient
D_4	side channel outer diameter	Φ_D	turbulent dissipation rate
D_5	balance cavity inner diameter	φ	channel wrap angle
D_6	balance cavity outer diameter	η	pump efficiency
F_1	axial force of the impeller	ρ	density of fluid

sealing ring and balance hole diameters to predict centrifugal pump axial force. Jin et al. (2022) established differential equations of motion for the axial self-balancing impeller in a centrifugal pump, examining its stability with the dynamic mesh technique and calculating the time required to reach a steady state under various conditions. Li et al. (2024a) studied the impact of floating impeller positioning on internal flow and axial force in vortex pumps with symmetric flow channels, noting that deviations from the central position reduce both head and efficiency. Yan et al. (2024) investigated and analyzed the internal flow field of an aviation fuel centrifugal pump under different operating conditions by numerical simulation and modified the theoretical equations of the axial force by combining them with the experimental results of force measurement. Li et al. (2024b) carried out a numerical simulation study on the axial force of desalination pumps and found that the axial force is closely related to the pump's operating condition, and it varies nonlinearly with the flow rate. Gu et al. (2024) examined the influence of axial oscillation frequency in a novel multistage centrifugal pump with a floating impeller using the dynamic grid technique. Their findings revealed that pressure fluctuations, efficiency, and the head coefficient exhibited periodic variations corresponding to the impeller vibration frequency, thereby increasing operational instability. Zhu et al. (2020) applied a global dynamic criterion algorithm to develop a BP neural network for optimising centrifugal pump efficiency and axial force under design conditions. Their results indicated that the optimised pump demonstrated reduced axial force and improved efficiency when operating under these conditions. Hu et al. (2022) proposed a multi-objective optimization strategy that combines computational fluid dynamics (CFD) numerical simulations, a genetic algorithm with back propagation (GABP) neural network, and the non-dominated sorting genetic algorithm III (NSGA-III). The results indicate that under rated clear water conditions, the optimized pump achieves a 14.65% reduction in shaft power and a 6.04% increase in efficiency, all while meeting the design requirements for the head. Jiang et al. (2025) combined machine learning with an improved NSGA-III algorithm to reverse-design the balance hole of a centrifugal pump impeller. They observed that optimisation enhanced head, efficiency, and shaft power while reducing axial force by 98.12%.

Existing research (Chen et al., 2022b; Wang et al., 2023; Yang et al., 2024, 2025) on vortex pumps has primarily focused on analysing internal flow mechanisms and optimising performance. However, studies investigating the effects of floating impeller deviations from the centre position in single-sided flow-channel vortex pumps remain limited, as do effective strategies for reducing axial force and improving pump stability in such systems.

In this study, the operational state of an impeller was simulated by adjusting the axial position of a floating impeller using numerical methods. The impact of axial displacement on the performance and axial force of a floating impeller in a single-sided flow-channel vortex pump was analysed. The results were evaluated in terms of the loss coefficients and static pressure distribution within the balancing cavity. Additionally, the effect of the balancing cavity on the axial force of the impeller under varying flow conditions was examined. The influence of axial displacement on the axial force of the vortex pump was clarified by simulating the axial position variations of the floating impeller. This study provides a theoretical basis for designing and optimising the hydraulic self-balancing structure of vortex pumps, offering valuable insights into improving axial force balance and enhancing the overall stability of vortex pump systems.

2. NUMERICAL MODEL AND METHODOLOGY

Figure 1 shows a schematic of the axial force balance structure in a single-stage vortex pump. In this study, a single-stage vortex pump with an axial inlet (CLDB240-768) was used. As illustrated, a hydraulic balancing method was employed to counteract the axial force between the two ends of the floating impeller. Grooves and balance cavities were designed to connect the high-pressure region. For clarity, the balance cavity near the pump inlet is referred to as the "inlet balance cavity," and the one near the outlet as the "outlet balance cavity." This naming convention was similarly applied to the inlet and outlet axial clearances. In this study, the inlet and outlet axial clearances were denoted as d_1 and d_2, respectively. In the vortex pump model, the inlet and outlet axial clearances were equal when the impeller was in the middle position. The designed dimensions of both axial clearances were 0.2 mm.

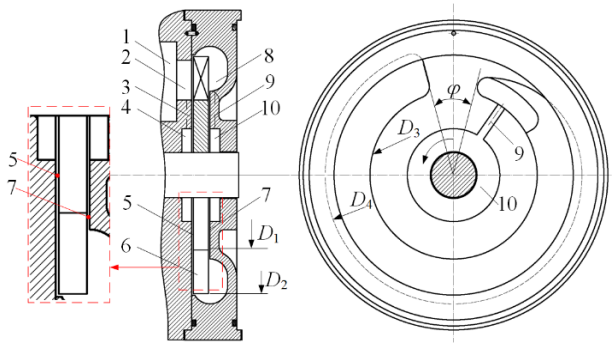

Note: 1. Inlet pipe; 2. Suction inlet; 3. Groove of the inlet balance cavity; 4. Inlet balance cavity; 5. Inlet axial clearance; 6. Impeller; 7. Outlet axial clearance; 8. Side channel; 9. Groove of the outlet balance cavity; 10. Outlet balance cavity.

Fig. 1 Single-stage vortex pump axial force balance structure diagram

Table 1 Parameters of vortex pump

Description	Parameter	value
Nominal flow rate of pump	Q_0 (m^3/h)	20
Nominal head	H (m)	50
Rotational speed	n_0 (r/min)	1450
Impeller inner diameter	D_1 (mm)	150
Impeller outer diameter	D_2 (mm)	240
Blade width	b (mm)	18
Number of blades	Z	24
Side channel inner diameter	D_3 (mm)	168
Side channel outer diameter	D_4 (mm)	258
Channel wrap angle	φ (°)	30
Balance cavity inner diameter	D_5 (mm)	47
Balance cavity outer diameter	D_6 (mm)	93
Designed inlet axial clearance	b_1 (mm)	0.2
Designed outlet axial clearance	b_2 (mm)	0.2

The working principle of the balance cavity is as follows: Owing to the asymmetrical flow channel in the vortex pump, impeller rotation causes an internal pressure rise, generating an axial force F_1 that acts on the impeller in the direction of the flow channel. Under the influence of this axial force, the impeller may undergo axial displacement towards the outlet. This reduces leakage in the outlet balance cavity, resulting in a gradual increase in local pressure. Concurrently, the pressure in the inlet balance cavity decreases as the end-face clearance widens, ultimately generating a restorative force F_2 that returns the impeller to its original clearance position relative to the casing.

The combined axial and restoring forces determine the new displacement of the impeller. By appropriately designing the size of the balance cavity and groove on both sides of the impeller, the impeller achieves dynamic balance near the equilibrium point where F_1=F_2. This prevents friction between the impeller and casing, ensuring the performance and operation of the pump remain unaffected.

The vortex pump features an open-type impeller and a closed-style centripetal channel in its structural design. The dimensions of the balance cavities and grooves on both sides of the impeller are identical. When the impeller is in the middle position, the axial and radial clearances on both sides are equal, each measuring 0.2 mm. The main parameters are detailed in Table 1.

2.1 Computational Domain

Figure 2 illustrates the computational fluid field of the single-stage vortex pump, which consists of seven main sections. Among these modifications, the inlet and outlet sections have been extended. Geometric treatment was applied to the sharp-cornered areas of the side channel. Furthermore, the impeller and clearances were treated as an integrated fluid field. The outlet balance cavity and side channel were combined into a single computational fluid domain, as were the axial clearances of the impeller and

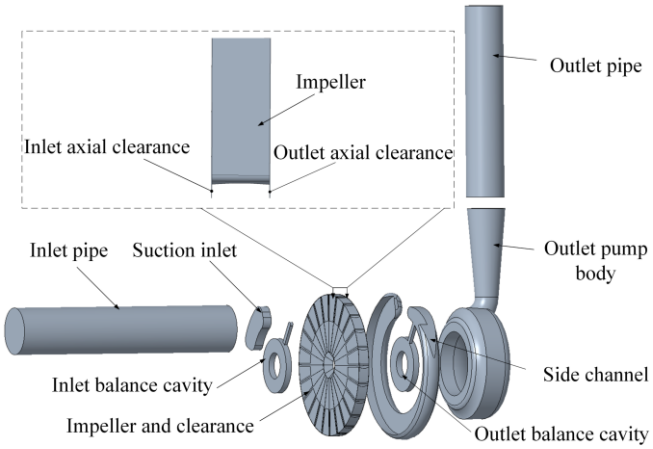

Fig. 2 Vortex pump computational fluid domain

the impeller itself. The inlet and outlet balance cavities of the vortex pump were symmetrically distributed on both sides of the impeller and had identical dimensions. Both cavities were connected to the high-pressure region inside the vortex pump through the grooves.

When the impeller is centred, the inlet (d_1) and outlet (d_2) clearances are both 0.2 mm. As the impeller moves, d_1 and d_2 change inversely, with a total floating range of 0.4 mm. Five sets of models were developed: d_1=0.1 mm (d_2=0.3 mm), d_1=0.15 mm (d_2=0.25 mm), d_1=0.2 mm (d_2=0.2 mm), d_1=0.25 mm (d_2=0.15 mm), and d_1=0.3 mm (d_2=0.1 mm). In this study, the floating impeller was positioned at five distinct axial locations by systematically adjusting the widths of the inlet and outlet axial clearances (ranging from 0.1 mm to 0.3 mm in 0.05 mm increments). All other geometric parameters, including blade geometry, flow channel dimensions, and the fluid domain configuration, were rigorously maintained to ensure consistency. This approach generated five unique vortex pump models, enabling a focused investigation into the effects of axial clearance variations on performance.

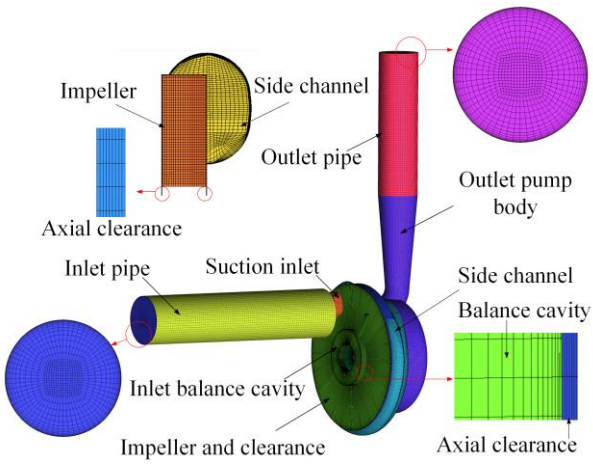

Fig. 3 Total mesh and mesh details

Table 2 Grid independence analysis

Test grids	1	2	3	4	5
Nodes ($\times 10^6$)	4.67	5.26	5.57	5.82	6.19
Head (m)	49.23	48.35	47.47	47.36	47.33
Efficiency (%)	31.1	30.2	29.89	29.86	29.85

2.2 Meshing Grid

Figure 3 presents a schematic of the total mesh and mesh details. As illustrated, the entire computational domain, except for the outlet pump body, employs a hexahedral-structured mesh. This includes the wall area of the boundary, clearance, and sharp corners of the side channel, which are locally encrypted for greater precision.

To improve the accuracy of flow field calculations in the clearance, the axial clearance on both sides of the impeller, measuring 0.2 mm in width, was divided into ten layers of mesh. Additionally, the balance cavity mesh adjacent to the clearance was encrypted to ensure a smooth transition from coarse to fine mesh. In this study, the minimum orthogonal quality and maximum skewness were 0.161 and 0.91, respectively, both of which fall within acceptable ranges.

The grid independence of the single-stage vortex pump was assessed under its rated operating status. As the number of grids increased, both the head and efficiency of this pump gradually decreased. It was observed that when the number of grids exceeded 5.57×10^6, the head and efficiency stabilised. This point represented the most economical number of grids, as detailed in Table 2.

2.3 Experimental and Numerical Verifications

The performance test bench for the vortex pump, shown in Fig. 4, primarily comprises a water tank, pipeline, vortex pump, power source, and control system.

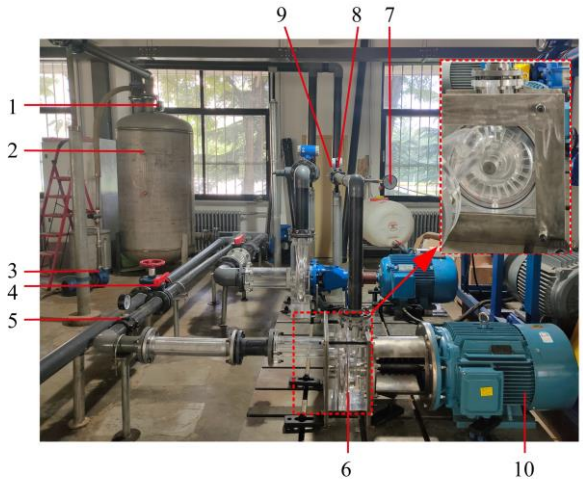

1.Vacuum meter; 2.Water tank; 3.Water ring vacuum pump; 4. Inlet valve; 5.Inlet pressure gauge; 6.Vortex pump; 7.Outlet pressure gauge; 8.Flow meter; 9.Outlet valve; 10.Motor.

Fig. 4 Schematic diagram of the experimental setup

Pressure gauges and flow meters were installed on the inlet and outlet pipelines to monitor variations in flow rate and pressure. A control valve was added to the outlet pipeline to regulate the flow rate.

During the experiment, the impeller was centered with a clearance of 0.2 mm at both ends, and measures were taken to ensure that the impeller remained axially stationary. 25 °C water served as the working medium, and five experiments were conducted for each operating condition.

This study employed the SST k-ω turbulence model, which is well-suited for numerically simulating flow in a vortex pump (Fleder & Böhle 2012). Water at 25 °C served as the working fluid for the simulation. The boundary conditions were set at the pressure inlet and mass flow outlet. No-slip wall boundary conditions were applied, along with standard wall functions near the walls. The pressure-velocity coupling was solved using the SIMPLEC algorithm. The basic equation set was discretised using the second-order upwind scheme for full-condition steady numerical simulation, with the convergence accuracy set to 10^{-5}. The mesh configuration satisfies the requirements of the turbulence model and the wall treatment method, resulting in a y+ value of less than 20. The average y+ value on the impeller blades was approximately 7, while on the side channel wall, it measured around 12. Both values fall within acceptable ranges, confirming the reliability of the numerical simulation results.

Steady numerical simulations were conducted, and the axial force was computed using the Force Report tool in FLUENT. This was achieved by integrating the pressure and viscous forces over the impeller's solid boundaries.

A comparison of the numerical simulation and experimental results for the vortex pump is shown in Fig. 5. The numerical simulation results and experimental

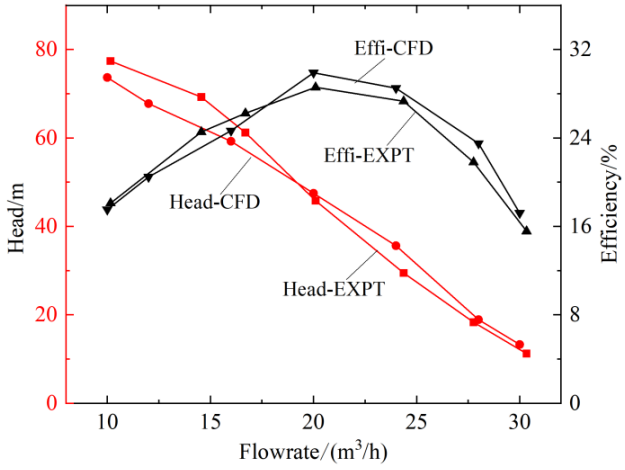

Fig. 5 Numerical simulation and experimental performance curve of vortex pump

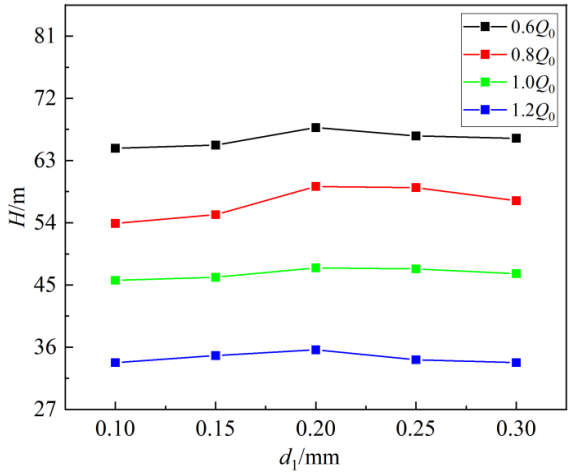

Fig. 6 Relationship curve of pump head and impeller axial position

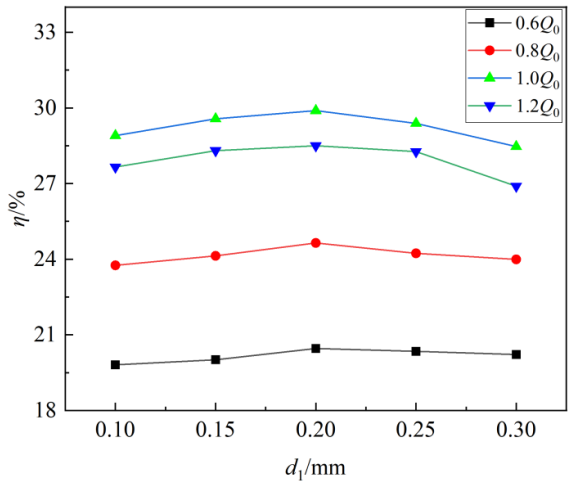

Fig. 7 Relationship curve of pump efficiency and impeller axial position

values closely matched the overall trend of the external characteristic curve and were consistent. The head of the vortex pump decreases with an increase in flow rate, while the pump efficiency initially increases and then decreases, reaching its maximum value at the rated operating point. The experimental results for this condition and the numerical simulation results showed an error of only 1.31%, with efficiency errors for other conditions also remaining within 5%. Under low-flow conditions, the simulation data exhibited relatively larger deviations from the experimental data. However, both the head and efficiency discrepancies stayed within the maximum error range of 5%, and the general trends were consistent. This confirms the reliability of the numerical methods and computational results presented in this study.

3. RESULTS AND DISCUSSIONS

3.1 Effect of Impeller Axial Displacement on Pump Head and Efficiency

The clearance within the vortex pump significantly affects its performance. Specifically, the outlet axial clearance adjacent to the side channel directly influences vortex pump performance (Zhang et al., 2015). To investigate how variations in the axial position of a floating impeller affect vortex pump performance, numerical simulations were conducted under various operating conditions with the impeller at different axial positions.

Figure 6 shows the influence curve of the impeller at various axial positions on the pump head. As illustrated, any deviation of the floating impeller from the central position results in varying degrees of reduction in the pump head. Specifically, greater deviation from the central position leads to a more significant reduction in head. Under designed conditions, reducing the inlet axial clearance to 0.1 mm decreased the pump head and efficiency by 3.81% and 0.99%, respectively, compared to the central position of the impeller.

As shown in Fig. 6, reducing the outlet axial clearance has a smaller impact on the pump head than reducing the inlet axial clearance, particularly under low-flow conditions. In a single-sided-channel vortex pump, the outlet axial clearance connects to the side channel, which is critical for energy transfer. While decreasing this clearance enhances energy transfer efficiency, it also increases the inlet axial clearance, worsening leakage and volumetric losses in that region. This results in a decrease in pump head. Therefore, only reducing the outlet axial clearance can improve the pump head.

Figure 7 illustrates the impact of the impeller's axial position on pump efficiency. The data indicate that when the floating impeller deviates from the central position, the pump efficiency declines to varying degrees. The greater the distance of this deviation, the more significant the reduction in efficiency. Additionally, the influence of the axial position on the head follows a consistent pattern. The effect of axial clearance at the outlet is less significant on efficiency compared to the inlet. As flow increases, the efficiency decline caused by the axial clearances at both the inlet and outlet become more consistent.

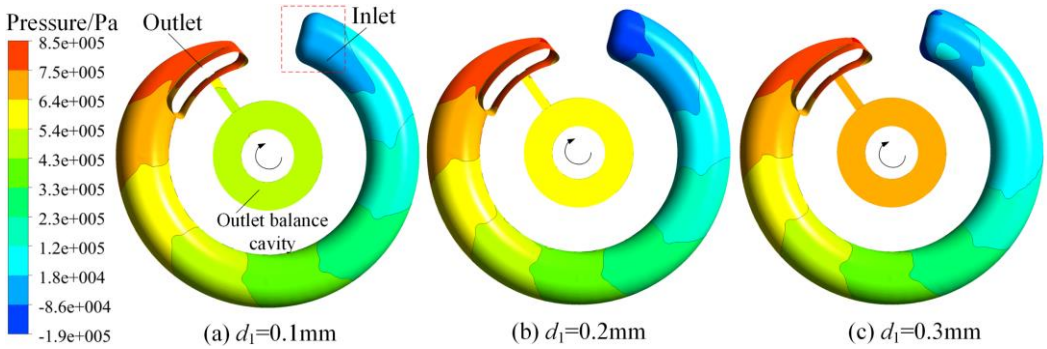

Fig. 8 Pressure nephogram of side channel at different axial positions of impeller under low-flow condition

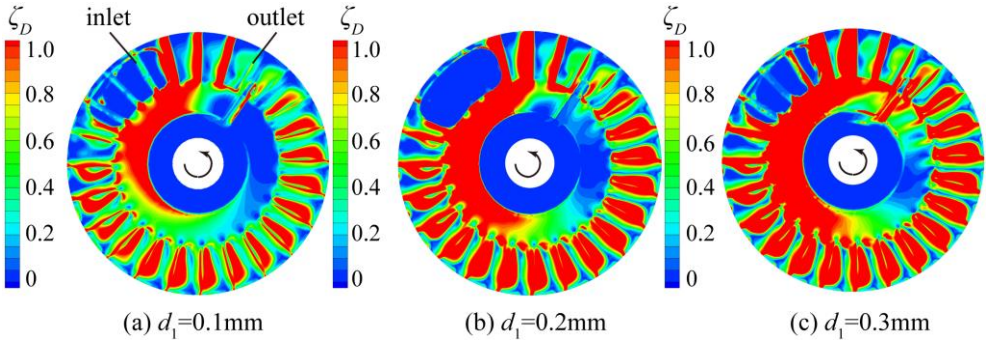

Fig. 9 Flow loss distribution with inlet axial clearance at different impeller axial positions

The constant change of the floating impeller axial displacement affects the pressure distribution in the balance cavity of the impeller, resulting in a larger flow loss, thus affecting the pump head and efficiency. From the simulation results, under different working conditions, the increase of the impeller axial displacement will lead to a gradual decrease in head and a slight decrease in efficiency, and the outlet axial clearance significantly affects the performance of the single-side channel vortex pump than the inlet axial clearance.

The numerical simulation results under low-flow conditions were selected for analysis. Figure 8 presents the pressure contour plots of the side channel in the vortex pump at different impeller axial positions under the $0.6Q_0$ operating condition. As illustrated, the pressure increases progressively along the direction of impeller rotation from the inlet to the outlet of the side channel, indicating continuous energy conversion between the impeller passages and the side channel, which results in pressure augmentation. The lowest pressure is observed in the inlet area. Specifically, when d_1=0.2 mm, the inlet pressure is minimised, and the pressure difference between the inlet and outlet is maximised, suggesting that the pump head reaches its peak at this axial position. Conversely, when d_1=0.1 mm, the pressure difference is minimised, and the pump head is also at its lowest, consistent with the results shown in Fig. 6.

Additionally, Figure 8 shows that the pressure in the outlet balance cavity increases with an increase in the inlet axial clearance d_1. This occurs because an increase in the inlet clearance reduces the outlet clearance, increasing the flow resistance between the outlet balance cavity and the flow channel, thereby elevating the pressure within the outlet balance cavity.

To further study the influence of axial clearances on the performance of the pump, the loss coefficient $\zeta_D=\Phi_D \cdot D_2^3/u_2^2\rho Q$ was introduced for analysis (Zhang et al. 2018), where Φ_D is the turbulent dissipation rate, D_2 is the outer diameter of the impeller, u_2 is the circumferential velocity at the impeller outlet, and ρ and Q is the fluid density and flow rate respectively. The flow loss in the vortex pump is primarily determined by turbulent dissipation. Therefore, the distribution of flow loss can be studied using the loss coefficient. The turbulent dissipation rate quantifies the conversion of kinetic energy into thermal energy within turbulent regions, indicating inefficiencies. Flow losses highlight the regions of energy dissipation that affect overall performance. The loss coefficient, obtained through a dimensionless treatment of the turbulent dissipation rate, increases with greater turbulent dissipation and flow loss.

Q_0 is the flow rate of the pump under the design condition. At the $0.6Q_0$ operating condition, a reduction in the inlet axial clearance has a greater impact on the performance compared to an increase in the inlet axial clearance. This specific operating condition was chosen for analysis because the vortex pump exhibits a higher head and lower efficiency at this flow rate, resulting in greater axial forces on the impeller.

Figure 9 illustrates the distribution of flow losses in the middle section of the inlet axial clearance under the $0.6Q_0$ operating condition. The figure shows that the flow losses are primarily concentrated in the low-pressure areas

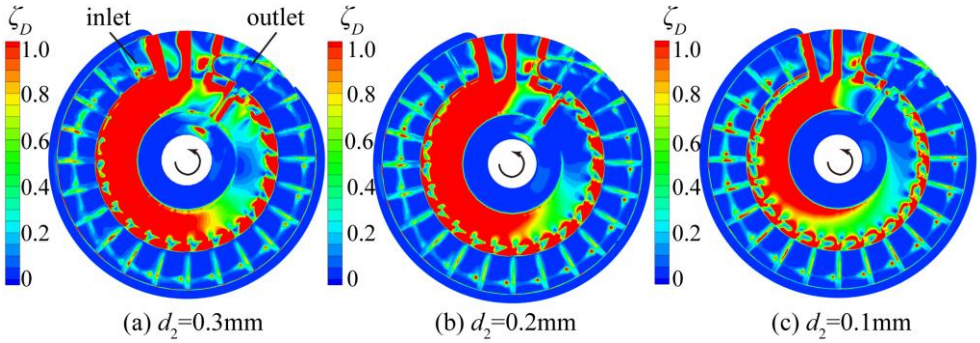

Fig. 10 Flow loss distribution with outlet axial clearance at different impeller axial positions

of the impeller passage and hub, whereas the flow loss in the inlet balance cavity region is relatively minor. As the inlet axial clearance increased progressively, the overall flow loss also increased. When the clearance increased from d_1 = 0.1 mm to d_1 = 0.2 mm, the flow losses in both the impeller passage and hub increased. From d_1 = 0.2 mm to d_1 = 0.3 mm, the increase in inlet axial clearance further escalated the leakage flow in the low-pressure area, causing an additional rise in flow loss within that region.

Figure 10 illustrates the distribution of flow loss in the middle section of the outlet axial clearance under the $0.6Q_0$ operating condition. It indicates that flow loss is primarily concentrated in the low-pressure region at the hub inlet and partially within the flow stability region. Additionally, significant flow loss occurs at the junction between the blade root and the side channel, attributed to a mismatch between the blade length and the height of the side channel. Notably, as the inlet axial clearance (d_1) increases and the outlet axial clearance (d_2) decreases, the overall flow loss of the outlet axial clearance is reduced.

A comparison of Fig. 9 and Fig. 10 reveals that flow losses in the inlet and outlet axial clearances are associated with the impeller's axial position. The side with greater clearance exhibits more significant flow loss, with the inlet axial clearance showing greater loss than the outlet axial clearance. An offset of the floating impeller from the central position increases the total flow loss across both axial clearances, leading to reduced head and efficiency. Due to the energy exchange between the outlet axial clearance and the side flow channel, reducing flow loss in this area enhances pump performance, particularly under low-flow conditions.

3.2 Effect of Impeller Axial Displacement on Axial Force

Unlike a fixed impeller, a floating impeller responds to a significant axial force by altering its pressure distribution due to axial displacement. This displacement helps to reduce the axial force, creating an interdependent relationship between the axial displacement and the axial force of the floating impeller. In this study, the direction of F_1 was defined as positive if it aligns with the direction of the pump inlet flow, and negative if it is opposite to that direction.

Figure 11 depicts the influence curve of different axial positions of the impeller on the axial force. When the

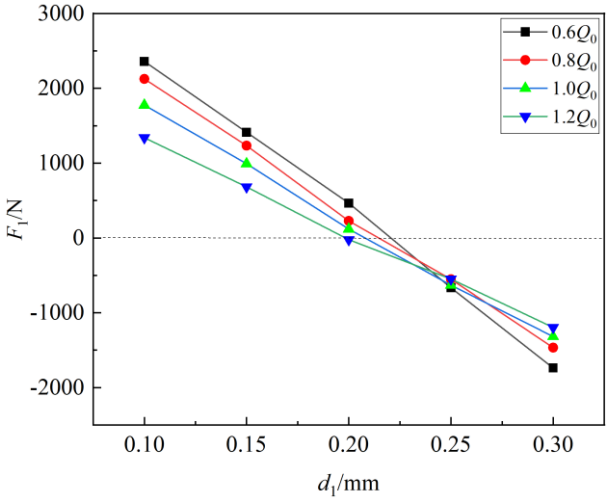

Fig. 11 Relationship curve of axial force and impeller axial position

impeller is in the middle position, the axial force is the smallest, and as the displacement increases, the axial force also increases. When the inlet clearance d_1 is less than 0.2 mm, the axial force points in the outlet direction, with smaller flow rates resulting in greater axial force. Conversely, when d_1 exceeds 0.2 mm, the axial force points in the inlet direction, with smaller flow rates again resulting in greater axial force. Due to the unbalanced design of the balance cavity, the axial force is smallest at the $1.2Q_0$ working condition.

As shown in Fig. 11, at flow rates of $0.6Q_0$, $0.8Q_0$, $1.0Q_0$, and $1.2Q_0$, the axial force is reduced by 15%, 10%, 8%, and 3%, respectively, when d_1= 0.2 mm. This indicates that changes in the axial position of the floating impeller significantly reduce the axial force.

As illustrated in Figure 11, the impeller attains a near-central position when the axial force approaches zero under rated operating conditions. Under such conditions, the influence of manufacturing tolerances on pump performance, including axial force, can be considered negligible, as supported by existing research (Zhuang et al., 2020) on manufacturing tolerances. However, under off-design conditions, the axial displacement of the impeller increases, and the impact of manufacturing tolerances—specifically geometric uncertainties—on

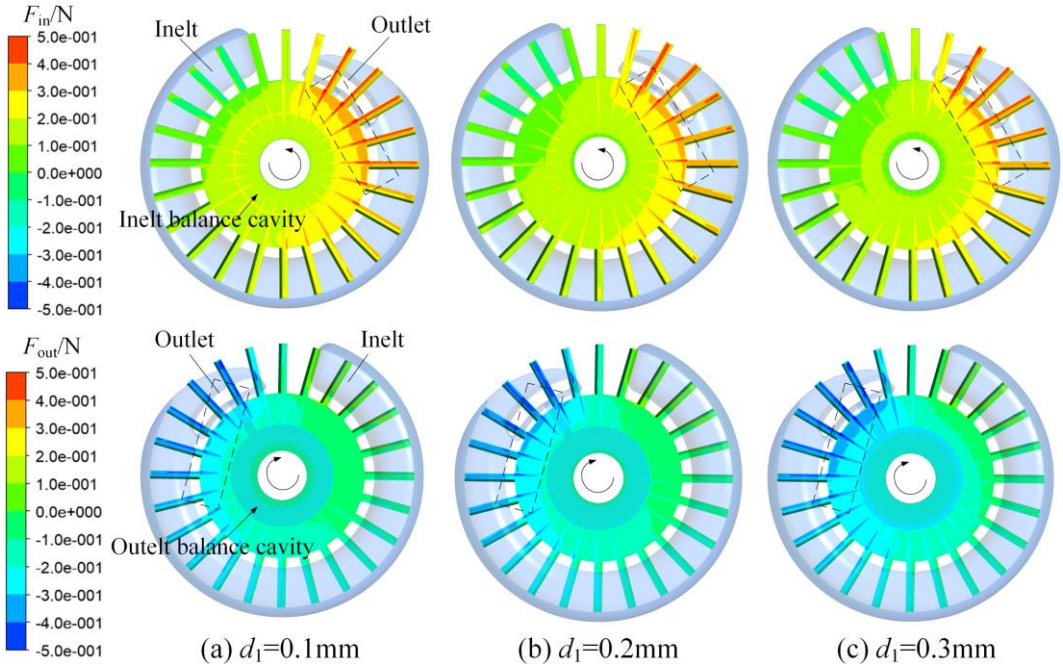

Fig. 12 Impeller axial force at different axial displacements under low flow conditions

Table 3 Axial force results under design flow at different impeller positions

Axial force	d_1=0.1mm	d_1=0.2mm	d_1=0.3mm
F_{in}/N	7961	7128	6634
F_{out}/N	-6186	-7010	-8028
F_1/N	1775	118	-1317

performance becomes significant and nonlinear (Wang et al., 2022). Further investigation is required to comprehensively validate these effects.

The axial force acting on the impeller of a vortex pump primarily originates from the fluid pressure differentials across the axial clearances at the inlet and outlet ends. To quantitatively analyze the axial forces on both sides of the floating impeller, we define the axial force exerted by the inlet clearance fluid as F_{in} and that from the outlet clearance fluid as Fout, with the resultant axial force $F_1 = F_{in} + F_{out}$. Three distinct impeller axial positions under rated operating conditions (Q_0=20m³/h) were investigated, with the corresponding numerical results presented in Table 3. Notably, positive force values indicate directions opposing the pump inlet, while negative values denote forces oriented toward the inlet.

As shown in Table 3, the inlet clearance consistently generated positive axial forces (F_{in}) that tended to displace the impeller toward the outlet side. Conversely, the outlet clearance produced negative axial forces (F_{out}) that drove the impeller toward the inlet side. As the inlet axial clearance d_1 progressively increased, F_{in} demonstrated systematic reduction, whereas F_{out} exhibited gradual intensification. This dynamic interaction causes the resultant axial force F_1 to transition from positive to negative values, indicating a reversal in the net force direction. This phenomenon reveals an essential self-regulating mechanism in floating impeller vortex pumps: When the impeller deviates from its central position, the resultant fluid pressure differential induces a spontaneous movement toward the region with larger axial clearance. This inherent feedback mechanism promotes dynamic equilibrium by automatically compensating for positional deviations.

To observe the distribution of axial forces on both sides of the floating impeller in the vortex pump, three axial displacement conditions (d_1 = 0.1 mm, d_1 = 0.2 mm, and d_1 = 0.3 mm) were selected under low-flow conditions ($0.6Q_0$) for analysis, where axial force exhibited the greatest variation. Figure 12 presents a cloud diagram showing the impeller's axial force distribution under varying axial displacements.

Figure 12 shows that the axial forces acting on the impeller are directed in opposite directions, both pointing toward the impeller surface. The axial force distribution increases circumferentially, with minimum values at the inlet and maximum values at the outlet.

By comparison, when d_1 = 0.1 mm, the axial force F_1 on the inlet side is greater than on the outlet side, causing

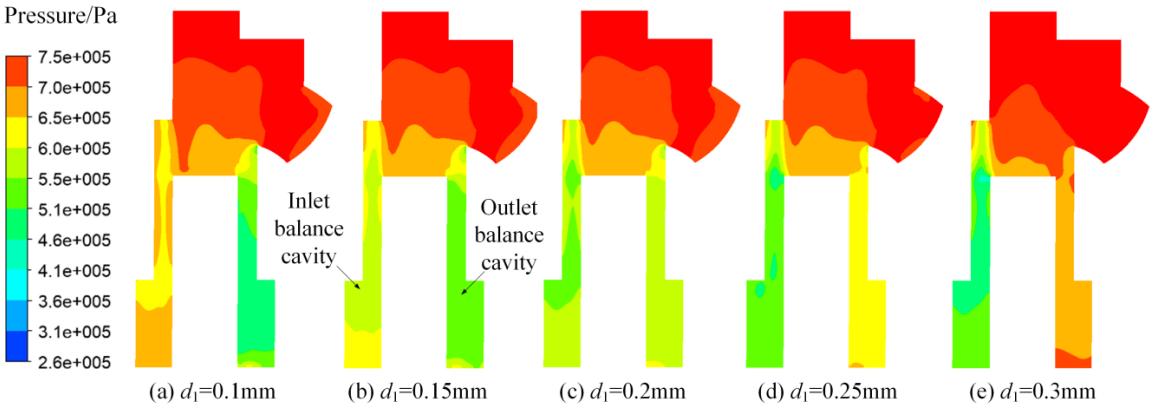

Fig. 13 Pressure distribution in balance cavities at various axial positions under low flow conditions

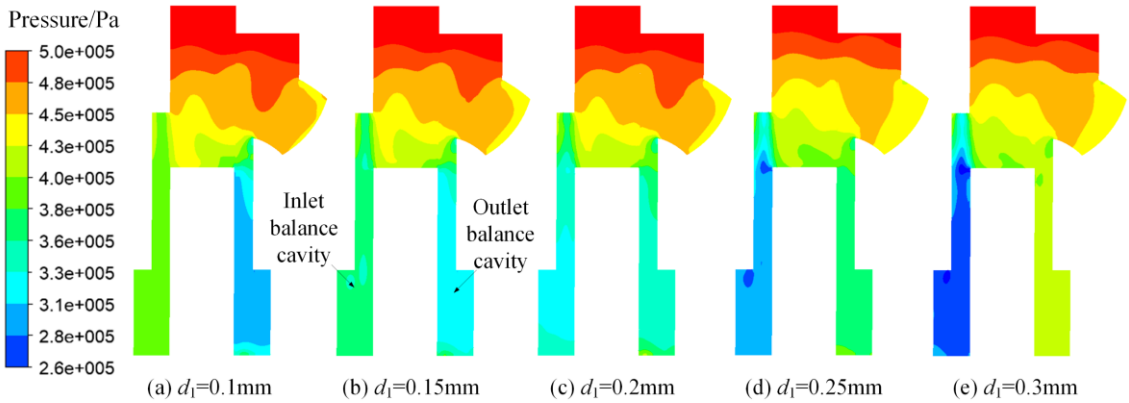

Fig. 14 Pressure distribution in balance cavities at various axial positions under high flow conditions

the resultant axial force to point toward the outlet side. This facilitates the impeller's return to a central position. Conversely, when d_1= 0.3 mm, axial force F_1 on the inlet side is less than that on the outlet side, resulting in the resultant axial force pointing toward the inlet side, which also aids in returning the impeller to the central position.

When the floating impeller is in the middle position (d_1=d_2=0.2 mm), the distribution of the axial forces and the difference in axial force values are the smallest. As shown in Fig. 12(b), the resultant axial force of the impeller reaches its minimum value. The axial force primarily originates from the difference in static pressure at both ends of the impeller.

The middle sections of the inlet and outlet balance cavities and grooves were selected to analyse the pressure changes. Figure 13 depicts the cloud diagrams of the pressure distribution at different axial positions under low flow conditions (0.6Q_0). The figure reveals that the static pressure in the impeller channel continuously increases along the radial direction, and the change in the axial position of the floating impeller has little influence on the static pressure distribution at the blade root. The static pressure in the inlet balance cavity decreases as the d_1 increases, while the static pressure in the outlet balance cavity increases accordingly.

When the impeller is in the middle position (d_1=d_2=0.2 mm), as shown in Fig. 13(c) the static pressure difference in the balance cavity on both sides is minimal. Therefore, when the floating impeller moves toward the inlet due to the axial force, the inlet axial clearance d_1 becomes smaller, increasing the pressure in the inlet balance cavity, while the pressure in the outlet balance cavity decreases. This generates a static pressure difference in the opposite direction of the axial force on both sides of the impeller, which helps restore the impeller to the middle position.

The pressure distribution in the balance cavity on both sides of the impeller at different axial positions under high flow conditions (1.2Q_0) is analysed for comparison, as illustrated in Fig. 14. The figure shows that the static pressure in the impeller channel increases radially. Specifically, the pressure in the inlet balance cavity decreases as d_1 increases, while the pressure in the outlet balance cavity increases. This pattern is consistent with observations made under low-flow conditions.

Compared with Fig. 13, it is evident that the static pressures in the balance cavity and impeller channel during high flow conditions are lower than those during low flow conditions. Consequently, when the floating impeller undergoes axial displacement, the pressure changes in the balance cavity are less significant than those under low-flow conditions. This results in a reduced balancing effect on the axial force.

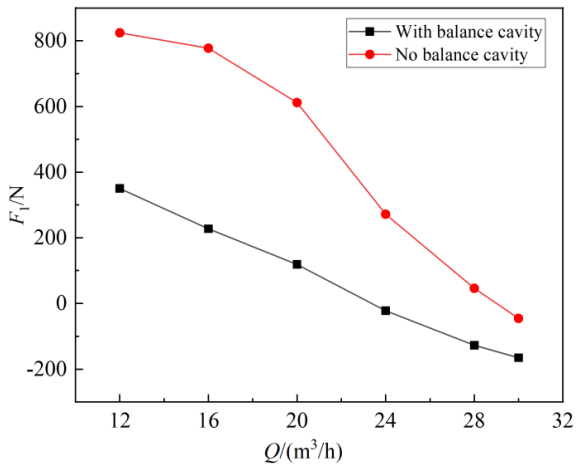

Fig. 15 Curves of axial force with and without balance cavity at different flow rates

Similarly, when the impeller is in the mid-position (d_1 = d_2 = 0.2 mm), as shown in Fig. 14(c), the static pressure difference between the two sides of the balance cavity is minimised. Compared to Fig. 13(c), the pressure distribution is more uniform, leading to a smaller difference in static pressure. Consequently, the axial force experienced by the impeller is lower than that under low-flow conditions.

Overall, changes in the axial position of the floating impeller have less effect on the pressure distribution within the impeller channel but significantly affect the flow in the cavities flanking the impeller. Thus, the effectiveness of the impeller's axial displacement in balancing its axial force diminishes as the flow rate increases.

3.3 Effect of Balance Cavity on Impeller Axial Force

The balance cavity plays a crucial role in altering the axial position of the floating impeller, thereby influencing the axial force acting on the impeller. The pressure of the liquid within the balance cavity determines the floating state of the impeller.

Optimising the design of the balance cavity is essential for achieving axial force balance in floating impeller vortex pumps. The change of the geometric size of the balance cavity, such as the diameter, will affect the sensitivity of the floating impeller to balance the axial force. The prototype diameter (93mm) of the balance cavity is reduced and increased to 80mm and 100mm respectively under the 0.6Q_0. Results show that the axial force on the impeller is increased to varying degrees, and the axial force corresponding to the diameter of 100mm is increased by 247N compared with the prototype design. Improving the structure of the balance cavity is key to addressing the issue of floating impeller jamming under off-design conditions.

To further study the mechanism of the balance cavity on the axial force of the floating impeller, the effect of the presence or absence of the balance cavity on the impeller in the intermediate position were analyzed. Figure 15 shows the influence curve of axial force with and without the balance cavity at different flow rates. It can be observed that the impeller axial force is reduced by 474 N, 550 N, 493 N, and 294 N under the action of the balance cavity at flow rates of 0.6Q_0, 0.8Q_0, 1.0Q_0, and 1.2Q_0, respectively.

This indicates that the balance cavity effectively reduces the axial force of the impeller. However, as the flow rate increases, the balancing effect of the balance cavity on the impeller axial force relatively decreases.

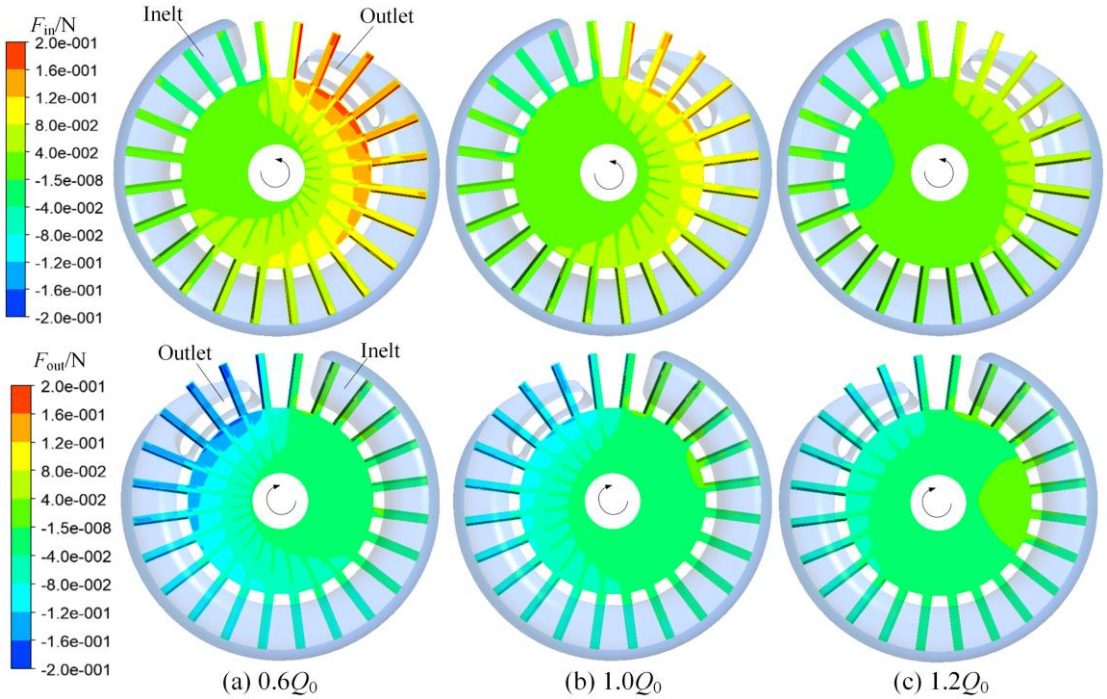

Fig. 16 Axial force distribution of the impeller without the balance cavity

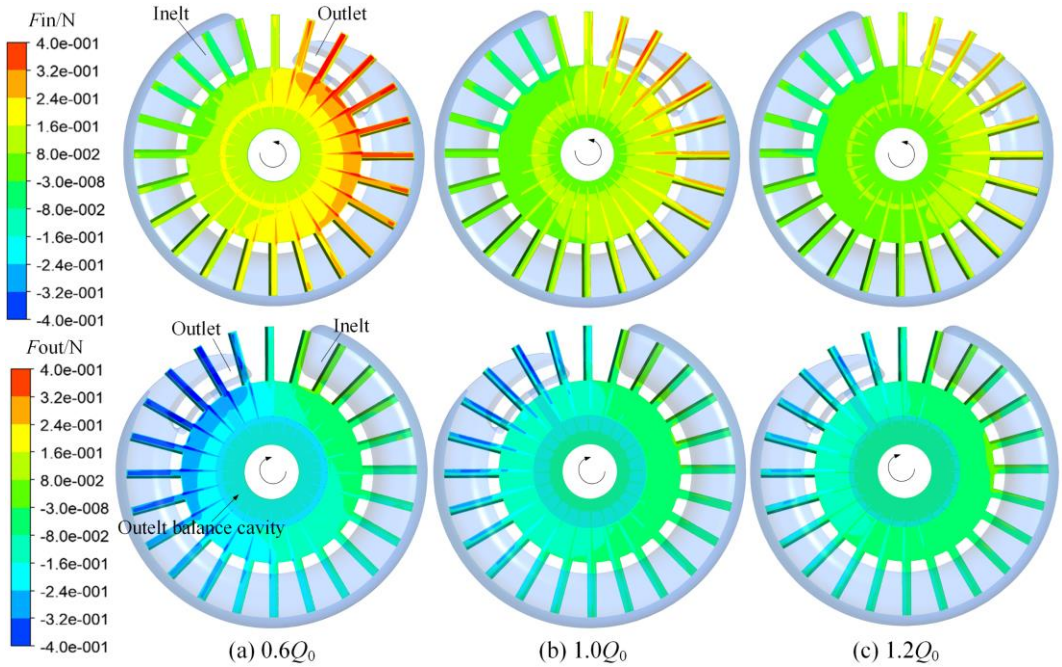

Fig. 17 Axial force distribution of the impeller under the action of the balance cavity

The effect of the balance cavity on axial force was investigated by comparing the axial force distributions of the impeller with and without the balance cavity. Fig. 16 presents the axial force distribution of the impeller in the absence of the balance cavity. The figure indicates that, without the balance cavity, the axial forces of the impeller increase progressively along radial and circumferential directions, with minimum values near the impeller inlet and maximum values near the outlet. The axial forces of the impeller act in opposite directions, both oriented toward the impeller surface.

As the flow rate increases, both the magnitude and distribution area of the axial force decrease, likely due to a reduction in the static pressure on the impeller. Overall, the resultant axial force tends to point toward the side channel, which is more pronounced under low-flow conditions.

Figure 17 illustrates the distribution of axial force of the impeller as influenced by the balance cavity. The figure reveals that, under low-flow conditions, the axial force near the exit of the high-pressure area increases in the radial direction, while the axial force in the inlet area and the balance cavity remains minimal.

Higher flow rates result in a marked reduction in axial force. This observation aligns with Fig. 15, which shows that at a flow rate of 1.2Q_0, the axial forces of the impeller effectively cancel each other out, reaching a minimum value under the influence of the balance cavity. Comparing Fig. 16 and Fig. 17, it is evident that the presence of the balance cavity alters the distribution of the impeller's axial force. While the balance cavity, connected to the high-pressure zone, increases the axial force due to the higher static pressure within the cavity, it also leads to a more uniform distribution of axial force near the exit of the high-pressure zone. As a result, this leads to a decrease in the total axial force.

Even at higher flow rates, the balance cavity continues to significantly impact fluid dynamics in the high-pressure region. This effect suggests that the balance cavity effectively reduces the pressure differential between hubs on either side of the impeller, especially in high-pressure areas, thereby helping to minimize axial force.

4. CONCLUSIONS

This study conducted numerical simulations and analyses to determine the influence of the axial displacement of a floating impeller on pump performance. The effects of the axial displacement of the floating impeller and the balance cavity on the impeller's axial force were analyzed, the conclusions are as follows:

(1) The axial displacement of the floating impeller significantly affects the pump's head and efficiency. As the axial displacement increases, the pump head and efficiency decrease, with greater flow losses occurring on the side where the axial clearance widens. Under the design working conditions, when the inlet axial clearance is reduced to 0.1 mm, the pump's head and efficiency decrease by 3.81% and 0.99%, respectively, compared to when the impeller is in the center position. Compared to the inlet axial clearance, reducing the outlet axial clearance has a relatively minor effect on the pump head. To optimize pump performance, it is crucial to maintain a smaller axial displacement and reduce the outlet axial clearance.

(2) At lower flow rates, the static pressure difference across the balance cavity on either side of the floating impeller increases, resulting in a higher axial force. Adjusting the axial position of the floating impeller can effectively reduces this axial force. At flow rates of 0.6Q_0, 0.8Q_0, 1.0Q_0, and 1.2Q_0, the axial force of the impeller is

reduced by 15%, 10%, 8%, and 3% respectively when d_1= 0.1 mm compared to d_1= 0.2 mm. The self-balancing axial movement of the floating impeller helps restore it to its central position, thereby minimizing the axial force on the impeller.

(3) The balance cavity alters the static pressure distribution in the high-pressure region, where extreme axial forces occur, effectively reducing the axial load on the impeller. As the flow rate increases, the static pressure in the balance cavity decreases, weakening its effect on the axial force.

ACKNOWLEDGEMENTS

This work was supported by the Gansu Major Scientific and Technological Special Project (Grant No. 23ZDGH001), the Central Government Guides Local Science and Technology Development Fund Projects (Grant No. 23ZYQA0320), and the Excellent Doctoral Program of Gansu Province (Grant No. 22JR5RA236).

CONFLICT OF INTEREST

The authors declare that they have no known competing financial interests or personal relationships that could have appeared to influence the work reported in this study.

AUTHORS CONTRIBUTION

Weifeng Yang: Writing-original draft, Investigation, Conceptualization, Data curation. **Renhui Zhang**: Writing-review & editing, Supervision, Methodology, Project administration, Funding acquisition. **Xiaoyuan Wang**: Writing-review & editing. **Guangqiang Guo**: Writing-review & editing.

REFERENCES

Adu-Poku, K. A., Zhang, F., Appiah, D., Chen, K., Osman, F. K., & Acheaw, E. (2022). Study on the inner flow mechanisms and unsteady force distribution of side channel pump. *Proceedings of the Institution of Mechanical Engineers, Part A: Journal of Power and Energy*, *236*(6), 1109–1128. https://doi.org/10.1177/09576509221081618

Chen, Q., Huan, Y. L., Peng, Q. Z., Xin, Y. C., & Hui, N. C. (2022a). Flow mechanism and axial force distribution characteristics of multistage pump cavity. *Science Progress*, *105*(4), 368504221145575. https://doi.org/10.1177/00368504221145575

Chen, K., Zhang, F., Appiah, D., Yuan, S., Hong, F., Zhu, L., & Song, M. (2022b). Effect of blade tip cutting angle on energy conversion mechanism of side channel pumps. *Physics of Fluids*, *34*(2), 025107. https://doi.org/10.1063/5.0082671

Fleder, A., & Böhle, M. (2012, September). *Numerical and experimental investigations on the influence of the blade shape on industrial side channel pumps*. *International Rotating Equipment Conference* (pp. 289-298).

Gantar, M., Florjancic, D., & Sirok, B. (2002). Hydraulic axial thrust in multistage pumps—origins and solutions. *Journal of Fluids Engineering*, *124*(2), 336–341. https://doi.org/10.1115/1.1454110

Gu, Y., Bian, J., Wang, Q., Stephen, C., Liu, B., & Cheng, L. (2024). Energy performance and pressure fluctuation in multi-stage centrifugal pump with floating impellers under various axial oscillation frequencies. *Energy*, *307*, 132691. https://doi.org/10.1016/j.energy.2024.132691

Guan, X. F. (2011). *Modern pump theory and design*. China Astronautic Publishing House.

Hu, Q., Zhai, X., & Li, Z. (2022). Multi-objective optimization of deep-sea mining pump based on CFD, GABP neural network and NSGA-III algorithm. *Journal of Marine Science and Engineering*, *10*(8), 1063. https://doi.org/10.3390/jmse10081063

Jia, Z. M. (1993). *Vortex pump, liquid ring pump, jet pump*. China Machine Press.

Jin, F. Y., Tao, R., Zhu, D., & Xiao, R. F. (2022). Stability of the axial-auto-balanced impeller of centrifugal pump. *Journal of Hydrodynamics*, *34*(4), 665-680. https://doi.org/10.1007/s42241-022-0060-1

Li, Q. Q., Tang, D. L., Ge, J., Lu, Y., Bie, F. F., & Zhu, X. Q. (2024a). Effect of floating impeller on the inner flow characteristics and axial force in regenerative flow pump. *Journal of Mechanical Engineering*, *60*(14), 378–386. https://doi.org/10.3901/JME.2024.14.378

Li, W., Song, R., Wang, Y., Ji, L., Li, S., Ye, X., ... & Agarwal, R. (2024b). Research on axial force and energy balance of seawater desalination high-pressure pump-based whole flow field numerical calculation. *Iranian Journal of Science and Technology, Transactions of Mechanical Engineering*, *48*(1), 29-47. https://doi.org/10.1007/s40997-023-00642-0

Liu, Z. L., Jia, X., Zhang, S., Shi, F. X., & Sun, Y. (2014). Influence of impeller axial displacement on liquid pressure in centrifugal pump chamber. *Journal of Lanzhou University of Technology*, *40*(6), 65-69. https://doi.org/10.13295/j.cnki.jlut.2014.06.016

Liu, Z. L., Wu, J., Zeng, J. L., Zhang, S., & Sun, Y. (2015). Influence of axial displacement of floating impeller on pump hydraulic performance. *Journal of Lanzhou University of Technology*, *41*(2), 51-54. https://doi.org/10.13295/j.cnki.jlut.2015.02.011

Liu, Z. L., Xu, L. Z., Jia, X., Wu, J., & Wang, D. W. (2013). Analysis of liquid flow and axial force calculation in axial clearance for floating impeller of centrifugal pump. *Transactions of the Chinese Society of Agricultural Engineering*, *29*(12), 79–85. https://doi.org/10.3969/j.issn.1002-6819.2013.12.011

Pehlivan, H., & Parlak, Z. (2019). Investigation of parameters affecting axial load in an end suction

centrifugal pump by numerical analysis. *Journal of Applied Fluid Mechanics*, *12*(5), 1615–1627. https://doi.org/10.29252/jafm.12.05.29623

Raheel, M. M., & Engeda, A. (2005). Systematic design approach for radial blade regenerative turbomachines. *Journal of Propulsion and Power*, *21*(5), 884–892. https://doi.org/10.2514/1.1426

Wang, X., Wu, Y., Wu, C., Wu, P., Yang, S., & Wu, D. (2024). Axial force balance method for floating impeller of shielded centrifugal pump. *Journal of ZheJiang University (Engineering Science)*, *58*(8), 1577–1584. https://doi.org/10.3785/j.issn.1008-973X.2024.08.005

Wang, X., Yao, L., & Zou, Z. (2022). Effect of loading level and axial distribution on uncertainty performance of turbine blade with geometric variations. *Aerospace Science and Technology*, *129*, 107851. https://doi.org/10.1016/j.ast.2022.107851

Yan, S., Kan, Y., Li, X., Xiao, L., & Ye, Z. (2024). Numerical calculation and experimental study of the axial force of aero fuel centrifugal pumps. *Applied Sciences*, *14*(10), 4313. https://doi.org/10.3390/app14104313

Yang, W. F., Zhang, R. H., Yang, H. D., & Chen, X. B. (2024). Energy conversion characteristics of flow in vortex pump based on vortex analysis. *Transactions of the Chinese Society for Agricultural Machinery*, *55*(5), 167–175. https://doi.org/10.6041/j.issn.1000-298.2024.05.015

Yang, W., Zhang, R., Wang, X., & Guo, G. (2025). Cavitation-induced variations in vortex structure and energy conversion dynamics in a vortex pump. *Energy*, *317*, 134478. https://doi.org/10.1016/j.energy.2025.134478

Zeng, J. L., Liu, Z. L., Huang, Q., Quan, H., & Shao, A. C. (2022). Research on the modified mathematical prediction model of impeller cover side cavity liquid pressure for centrifugal pumps. *Journal of Applied Fluid Mechanics*, *15*(3), 673–685. https://doi.org/10.47176/jafm.15.03.33327

Zhang, F., Böhle, M., Pei, J., Yuan, S., & Fleder, A. (2015). Numerical simulation and verification on flow characteristics of impeller axial and radial gaps in side channel pump. *Transactions of the Chinese Society of Agricultural Engineering*, *31*(10), 78–83. https://doi.org/10.11975/j.issn.1002-6819.2015.10.011

Zhang, F., Yuan, S. Q., Wei, X. Y., & Chen, K. (2018). Study on Flow Loss Characteristics of Side Channel Pump Based on Entropy Production. *Chinese Journal of Mechanical Engineering*, *54*(22), 137–144. https://doi.org/10.3901/JME.2018.22.137

Zhao, W. G., He, M. Y., Qi, C. X., & Li, Y. B. (2013, December). *Research on the effect of wear-ring clearances to the axial and radial force of a centrifugal pump.* IOP Conference Series: Materials Science And Engineering (Vol. 52, No. 7, p. 072015). IOP Publishing. https://doi.org/10.1088/1757-899X/52/7/ 072015

Zhu, D., Xiao, R., Yao, Z., Yang, W., & Liu, W. (2020). Optimization design for reducing the axial force of a vaned mixed-flow pump. *Engineering Applications of Computational Fluid Mechanics*, *14*(1), 882-896. https://doi.org/10.1080/19942060.2020.1749933

Zhuang, H. W., Teng, J. F., & Zhu, M. M. (2020). Impacts of blades considering manufacturing tolerances on aerodynamic performance of compressor. *Journal of Shanghai Jiao Tong University*, *54*(09), 935-942. https://doi.org/10.16183/j.cnki.jsjtu.2020.150